(4)

AR-005-733

SIMULATION OF SEDIMENTATION BY MOLECULAR DYNAMICS

Rodney A.J. Borg

MRL Research Report
MRL-RR-7-89

ABSTRACT

A study of sedimentation processes of macroscopic, spherical particles using a molecular dynamics simulation was undertaken. Calculations were performed on particles of 30, 50 and 100 μm radius. For particle size distributions where all of the particles have the same radius (monomodal) it was found that the density of the sediment is always less than the density of an equivalent close packed structure. In addition, an increase in particle radius leads to a decrease in the sediment density. For bimodal particle size mixes, either 30/50, 50/100 or 30/100 μm radii, fractionation was found to occur. In all cases, the larger particles settled before the smaller particles giving rise to a layer of small particles on the top of the sediment, and a higher number ratio of larger particles in the lower portions.

Published by DSTO Materials Research Laboratory
Cordite Avenue, Maribyrnong, Victoria 3032, Australia
Telephone: (03) 319 3887
Fax: (03) 318 4536

AR No. 005-733

Approved for public release

AUTHOR

Rodney Borg was born in Melbourne in 1965 and graduated BSc (Hons) in Chemistry from the University of Melbourne in 1987. He joined MRL in 1988 as an Experimental Officer with the Explosives Division. He is currently a Cadet Research Scientist studying towards a PhD at the Flinders University of South Australia where his research work is concerned with the study of molecular photodissociation by vector correlations.

CONTENTS

SIMULATION OF SEDIMENTATION BY MOLECULAR DYNAMICS

1. INTRODUCTION

Composition B is a widely used military explosive that is a 60/40 RDX/TNT mixture. Typically, ordnance is filled by a casting process whereby Composition B is heated above the melting point of TNT, then poured into the ordnance shell and allowed to cool and solidify. The Composition B mixture is typically heated 10-20°C above the melting point of TNT (ca 80°C), i.e. well below the melting point of RDX (ca 205°C) which decomposes at its melting point. At these temperatures, the solubility of RDX in TNT is 5-6 wt% [1] hence this heated mixture is essentially a suspension of solid RDX particles in liquid TNT.

Sedimentation of RDX can therefore occur during cooling and solidification of the TNT. Because batches of RDX have a wide particle size distribution, fractionation can occur during sedimentation. RDX is generally more sensitive to initiation than TNT, and therefore the fractionation process will produce localised regions of higher RDX content, hence higher sensitivity. An understanding of sedimentation processes will aid the production of Composition B products and other RDX based explosives where sedimentation can occur, helping to optimise homogeneity of fills using these explosives.

In this report, a computer simulation technique was used to study sedimentation processes. Since the forces exerted on a particle in a suspension can be described readily, the method of Molecular Dynamics (MD) is particularly suitable. In MD calculations, the forces on all particles are calculated and then the particles are moved according to Newton's equations of motion. This process develops from an initial state of particles dispersed in a viscous medium subject to gravity and the calculation is continued until some final state is reached; in this case the final state is complete sedimentation. In the calculations, this is assumed complete when none of the particles has significant motion.

One of the more interesting aspects of sedimentation is the effect of particle size distribution on the final density of the sediment. Information gained on this effect can be used to tailor particle size distribution so as to obtain a required sediment density.

2. MOLECULAR DYNAMICS (MD) THEORY

2.1 Overview

In MD calculations (see [2] for a review), particles are moved according to Newton's equations of motion [3], after the forces on the particles have been evaluated. This process of force evaluation/movement is repeated in cycles until the final state is achieved. Consequently, the major features of an MD code are:

(i) The force computation.
(ii) Solution of Newton's equations of motion.

For computational convenience (see later), the force calculation and solution of the equations of motion are not completely separated. Some form of "container" is needed to describe the space occupied by the particles. For sedimentation, a square beaker has been used where the X and Y directions correspond to the width and depth of the container. The Z direction is aligned with the direction of gravity and corresponds to the height of the container. In order to make this beaker behave like a real beaker, certain constraints are placed on the X,Y and Z directions and these constraints will be described in detail in section 2.2.

2.2 Force Calculation

The important forces in a sedimentation process are viscosity, gravity, interparticle forces, particle/floor forces and buoyancy.

The magnitude of the viscous force on a spherical particle is given by [4]:

$$\mathbf{F}_v = -6\pi\eta r_i \mathbf{v}_i \qquad (1)$$

where η is the liquid phase viscosity, r_i is the radius of particle i and $\mathbf{v}_i$ is the velocity of particle i. The viscous force acts in the direction opposite to the direction of the motion of the particle.

Gravitational force is given by:

$$\mathbf{F}_{ig} = m_i \mathbf{g} \qquad (2)$$

where m_i is the mass of the i'th particle and $\mathbf{g}$ is the gravitational field strength. In the present calculations, the gravitational force is defined as being in the -Z direction (i.e. $\mathbf{g} = [0,0,g_z]$).

The interparticle forces describe the interaction between particles. Here, the particles are assumed to be spherical "soft" spheres. A "soft" sphere model is necessary to overcome numerical stability problems as well as reducing particle

overlap. There is no long-range attraction (e.g. opposite charge attraction) or cohesion/adhesion force. A truncated Lennard-Jones 12-6 type potential proved to be the most suitable and is given by:

$$\mathbf{F}_{ij} = 4\epsilon_{ij}\left(\frac{12\sigma_{ij}^{12}}{r_{ij}^{13}} - \frac{6\sigma_{ij}^{6}}{r_{ij}^{7}}\right)\hat{\mathbf{d}} \qquad (3)$$

where r_{ij} is the interparticle distance, ϵ_{ij} and σ_{ij} are constants for pair (i,j) and $\hat{\mathbf{d}}$ is a unit vector along the interparticle line. The direction of this force is along the interparticle vector. The range of $\mathbf{F}_{ij}$ is 0 to $r_i + r_j$, that is from zero to the sum of the particle radii, and for $r_{ij} > r_i + r_j$ we assume $\mathbf{F}_{ij} = 0$. This means the force starts to operate when the particles start to touch. See Figure 1 for a typical plot of this function.

In the simulation, there is a restriction on the number of particles that can be included because of the limitations imposed by the storage capabilities of the computer being used. Because of this limit, a technique called minimum imaging is employed to overcome undesirable edge effects. With minimum imaging, the box of particles being studied is surrounded by mirror images of itself in the X and Y directions. When interparticle forces are calculated between a pair (i,j), the i'th particle is deemed to be in the original box and the j'th particle is then chosen from the original or images such that the distance is a minimum. Another way of describing this is that a particle leaving the box in, say, the +X direction is treated as entering the box from the -X direction. Thus minimum imaging also describes "periodic boundary conditions".

A particle-floor potential is needed between the particles and the bottom of the container. The form of this potential was taken as:

$$\mathbf{F}_i^{floor} = \frac{K_i}{r_i^{floor\,13}}\hat{\mathbf{k}} \qquad (4)$$

where r_i^{floor} is the distance between particle i and the bottom of the container, K_i is a constant for particle type i and $\mathbf{k}$ is a unit vector in the Z direction. The form of this potential is basically the repulsive part of equation (3) and was chosen for consistency as well as its success in providing an adequate description of the bottom boundary. The range of $\mathbf{F}_i^{floor}$ is 0 to r_i, i.e. from zero to the particle radius, and for $r_i^{floor} > r_i$ we assume $\mathbf{F}_i^{floor} = 0$. Figure 2 gives a typical representation of this function. It should be noted that minimum imaging is not employed in the direction of gravity (i.e. the Z direction).

Strictly speaking, a buoyancy force should also be incorporated into the calculations. However, at this stage we are primarily interested in the way particles pack during sedimentation and less interested in rates of sedimentation. Including

buoyancy will only reduce the effect of gravity, since it operates in the exact opposite direction, and is not expected to affect the mode of packing. Consequently, buoyancy has been omitted from the calculations presented here.

The effect of Brownian motion on the sedimenting particles has not been included in the calculation as the particle sizes considered here are large enough for it to be neglected. A simple criterion for the neglect of Brownian motion is that the particle Peclet number be much larger than unity [5]. For the system considered here this will be the case provided the particle number is greater than 1 μm. The smallest particle radius considered here is 30 μm, hence Brownian motion has not been included in the calculation.

The total force on a particle is therefore given by:

$$\mathbf{F}_i = m_i \mathbf{a}_j = \sum_{\substack{j=1 \\ j \neq i}}^{N} \mathbf{F}_{ij} + m_i \mathbf{g} - 6\pi\eta r_i \mathbf{v}_i + \mathbf{F}_i^{floor} \qquad (5)$$

where N is the number of particles, $\mathbf{v}_i$ is the velocity and $\mathbf{a}_i$ is the acceleration of particle i.

2.3 Solving the equations of motion

For a molecular dynamics simulation, the velocity and position at one time step are related to the velocities and positions at other time steps via the Verlet equations [6]:

$$\mathbf{v}_i(t) = \frac{1}{2\Delta t} (\mathbf{r}_i(t + \Delta t) - \mathbf{r}_i(t - \Delta t)) \qquad (6)$$

$$\mathbf{r}_i(t + \Delta t) = 2\mathbf{r}_i(t) - \mathbf{r}_i(t - \Delta t) + \mathbf{a}_i(t)\Delta t^2 \qquad (7)$$

where $\mathbf{v}_i(t)$ is the velocity vector of particle i at time t, $\mathbf{a}_i(t)$ is the acceleration vector of particle i at time t and $\mathbf{r}_i(t)$ is the position vector of particle i at time t. To calculate $\mathbf{r}_i(t + \Delta t)$, $\mathbf{a}_i(t)$ must be known. From equation (5), for $\mathbf{a}_i(t)$ we need $\mathbf{v}_i(t)$ which, in turn, is dependent on $\mathbf{r}_i(t + \Delta t)$. This difficulty can be overcome as follows (considering only the x-component for one particle). Equation (5) can be written as:

$$\frac{d^2 x_n}{dt^2} = \frac{1}{m_i} \left(\sum F_{ijx} + m_i g_x + F_{ix}^{floor} \right) - \frac{6\pi\eta r_i}{m_i} \frac{dx_n}{dt} \qquad (8)$$

where x_n is the x-coordinate of particle i at time t. Since F_{ijx} and F_{ix}^{floor} are only dependent on the particle positions at time t (which are known) and $m_i g_x$ is a constant, equation (8) then becomes:

$$\frac{d^2x_n}{dt^2} = A - \alpha \frac{dx_n}{dt} \tag{9}$$

where

$$A = \frac{1}{m_i} \left(\sum F_{ijx} + m_i g_x + F_{ix}^{floor} \right) \tag{10}$$

$$\alpha = \frac{6\pi\eta r_i}{m_i} \tag{11}$$

Equation (7) can be written as (x-component only):

$$x_{n+1} = 2x_n - x_{n-1} + \frac{d^2x_n}{dt^2} \Delta t^2 \tag{12}$$

where x_{n+1} is the particle x-coordinate at time $t + \Delta t$ and x_{n-1} is the particle x-coordinate at time = $t - \Delta t$. Equation (6) can then be simplified using equations (9) and (12):

$$\begin{aligned} \frac{dx_n}{dt} &= \frac{1}{2\Delta t} (x_{n+1} - x_{n-1}) \\ &= \frac{1}{2\Delta t} \left(2x_n - 2x_{n-1} + \frac{d^2x_n}{dt^2} \Delta t^2\right) \\ &= \frac{x_n - x_{n-1}}{\Delta t} + \frac{\Delta t}{2} \frac{d^2x_n}{dt^2} \\ &= \frac{x_n - x_{n-1}}{\Delta t} + \frac{\Delta t}{2} A - \frac{\alpha \Delta t}{2} \frac{dx_n}{dt} \end{aligned} \tag{13}$$

Collecting dx_n/dt on the RHS gives:

$$\frac{dx_n}{dt} = \frac{1}{(1 + \alpha(\Delta t/2))} \left(\frac{x_n - x_{n-1}}{\Delta t} + \frac{\Delta t}{2} A\right) \tag{14}$$

Equation (14) can be evaluated given x_n and x_{n-1} only. Initially, particle positions and velocities are assigned then x_1 is approximated via :

$$x_1 = x_0 + \frac{dx_0}{dt} \Delta t \qquad (15)$$

Subsequent MD cycles follow the sequence below:

1/ Evaluate A using equation (10)
2/ Solve equation (14) giving the particle velocities dx_n/dt
3/ Solve equation (9) giving the particle accelerations d^2x_n/dt^2
4/ Solve equation (12) giving x_{n+1}
5/ Increase the time step by an increment
6/ Start again at step 1.

In this scheme, the force evaluation and solution of the equations of motion are interleaved to overcome the velocity dependence of the force.

One further point to note is the use of periodic boundary conditions in the X and Y directions, as discussed in Section 2.2. If a particle moves outside of the X or Y limits of the container it is removed and replaced by an identical particle (with the same velocity vector) entering the container from the opposite side.

3. VOLUME CALCULATIONS

In order to compare results for different particle size distributions, a method for calculating the sediment volume is required. Given the box dimensions, the particle coordinates and radii, the volume can be calculated by evaluating the volume under the top surface of the particles. The top surface can be defined by lowering a grid of small squares onto the sediment until all of the squares have intersected a particle (Figure 3). The volume is then the sum of the volumes under every square, and shall be called V_{MD} for volume from molecular dynamics calculation. For comparison, we define two other volumes:

$$V_s = \frac{4\pi}{3} \sum_{i=1}^{N} r_i^3 \qquad (16)$$

$$V_c = 4\sqrt{2} \sum_{i=1}^{N} r_i^3 \qquad (17)$$

V_s corresponds to the total volume of the spheres only and ignores any interstices created when spheres pack together. V_c is the close packed volume for either HCP (hexagonal close packing) or FCC (face centered cubic). It is expected that:

$$V_{MD} \geq V_c > V_s$$

so V_c and V_s provide a check on the V_{MD} value. If V_{MD} is equal to V_c then the particles must be close packed. The use of V_c is only meaningful for situations where all the particles are the same size.

The density of the sediment, ρ_{MD}, is given by:

$$\rho_{MD} = \frac{\Sigma_{i=1}^{N} m_i}{V_{MD}} = \frac{(4\pi\rho_o) \Sigma_{i=1}^{N} r_i^3}{V_{MD}}$$

$$\rho_{MD} = \frac{V_s}{V_{MD}} \rho_o \qquad (18)$$

where m_i is the mass of the i'th particle and ρ_o is the particle material (crystal) density.

When comparing results where the only difference is the particle size distribution, we can define a relative density:

$$\rho_r = \frac{\rho_{MD}}{\rho_o} = \frac{V_s}{V_{MD}} \qquad (19)$$

ρ_r must be ≤ 1, and in general will be significantly less than unity. The nearer to unity it becomes, the more closely packed is the sediment.

4. RESULTS

4.1 Computational considerations

One of the less desirable features of a molecular dynamics code is its order N usage of CPU time where N is the number of particles in the simulation. This means that an increase in the number of particles by a factor of two will give a factor of four increase in the CPU time needed to perform the simulation. It is possible to write MD codes that give improved performance [7] but these are more complicated and take longer to develop. Since it was not clear if order N performance would be prohibitive, the extra effort to write a more efficient code was not undertaken.

Apart from changing the basic algorithm used in the MD code, improvements in time efficiency can be obtained by implementing other innovations. In this work, the interparticle and particle/floor forces are tabulated. This removes the time expensive process of r^{13} and/or r^{12} evaluation every time the force is calculated and replaces it with a look-up table. Interpolation is not necessary due to the high resolution of the look-up table. The Δt used in Equations (6) and (7) can be increased to reduce the number of cycles needed for complete sedimentation. However, if Δt is increased too much the calculation can become unstable. This instability arises from excessive particle motion in a given cycle. The large motions lead to excessive particle overlap which in turn cause huge forces on the overlapping particles that finally leads to particle movements many times the size of the box dimensions. Such movements cannot be handled adequately and lead to numerical problems. Consequently, Δt must be chosen very carefully to avoid instabilities yet allow as few cycles as possible for complete sedimentation. The severity of this instability problem can also be influenced by the choice of interparticle potential.

Initially, the particles are placed randomly within a box and given a random velocity. To obtain statistically meaningful results, calculations should be performed a number of times with different initial conditions. The pseudo random number generator used to provide these initial conditions is based on the recurrence relation [8]:

$$p(i) = Ap(i-1) \bmod M \qquad (20)$$

where p(i) is the i'th pseudo random number generated, M is the period of the pseudo random number generator and A is a constant. The p(i) are distributed between 0 and M. Therefore to obtain random numbers between 0 and 1 all that is required is division by M.

In addition, instead of using the viscosity of liquid TNT at an appropriate temperature, the viscosity of water at 25°C ($\eta = 8.904 \times 10^{-2}$ Pa.s [9]) was used throughout the calculations. The reason for this comes back to computer time; TNT has a higher viscosity so more cycles are needed for complete sedimentation and hence more CPU time will be used. The particle material density was also given an arbitrary value of 2 Mg/m^3. This value doesn't reflect the density of any material in particular, but is a value that has the same order of magnitude as the density of typical explosive solids.

Values of ϵ and σ can be obtained in the literature [10] for atoms and molecules. However, ϵ and σ values for macroscopic particles like those used in this study are not readily available. The values used here have been chosen somewhat arbitrarily but satisfy the required conditions fairly well, i.e. the particles behave as "soft" spheres. K values are also assigned in a similar fashion. Tables 1, 2 and 3 list values of ϵ, σ and K used in this work. The results we obtained were found not to be sensitive to the choice of ϵ, σ or K.

4.2 All particles the same size (monomodal blend)

Initial calculations were performed for suspensions where all of the particles have the same radius. These results provide an indicator as to the reliability of the code as

well as providing a simple starting point for more involved calculations. Three particle sizes were investigated; r = 30, 50 and 100 μm (Tables 4, 5 and 6). In order to obtain statistically meaningful results, similar calculations were performed a number of times for each radius. The only difference between these calculations is the starting positions and velocities of the particles. Inspection of the ρ_r values (Table 7) for the three radii show that ρ_r tends to decrease slightly with increasing radius. This suggests that smaller particles tend to pack more closely than larger particles.

The size of the calculation, i.e. the number of particles, can have a marked affect on the results of MD calculations especially if periodic boundaries are not used. The size effect was investigated by repeating the 50 μm radius calculations with N = 216 (Table 8). There is no statistically significant difference in the V_{MD} value for N = 125 and N = 216. This indicates that N = 125 is sufficient to obtain reliable results for monomodal particle size distribution. Comparison of the average times for N = 125 and N = 216 demonstrate the order N^2 performance, $(216/125)^2 \approx 3$; one would therefore expect a factor of three increase in CPU time for the N = 216 run as compared to the N = 125 run. From Table 5, the N = 125 run takes about 42 minutes and from Table 8 the N = 216 run takes about 125 minutes so the expected time increase is the same as the observed time increase.

4.3 Particles of two sizes (bimodal blends)

Three mixes were investigated here, namely, 30/50, 50/100 and 30/100 μm mixes. The number ratio of the small to large particles was held fixed at 5:3. The results are presented in Tables 9, 10 and 11. With a mix, there is the possibility of fractionation occurring during sedimentation therefore plots of the probability of locating a particle centre as a function of height (in the Z direction) were obtained.* To improve the statistics of these plots, the final particle coordinates of all of the runs of a particular mix were combined and then analysed. The plots obtained are shown in Figures 4, 5 and 6.

The bimodal calculations were more susceptible to instability problems than the monomodal of section 4.2, requiring a smaller Δt in conjunction with more cycles for the simulations. In addition, the greater the difference in the particle size, the greater was this instability. One possible explanation for this lies in the relative terminal velocities of the particles. By considering the free fall of a particle in the suspension (free fall here means there are no interparticle or particle/floor forces on the particle) it can be shown that the terminal velocity of a particle is proportional to the square of the particle radius. Thus, larger particles move with a higher velocity and will move greater distances in a given cycle than smaller particles. It would then seem possible, within a single time step, for a large particle to considerably overlap a smaller particle.

---

* In fact, sedimentation is a well-known technique for particle sizing measurements [11].

5. DISCUSSION

The most important parameter calculated for this study was V_{MD}, and it was important to ensure that enough independent estimates were obtained to provide a representative sample. To gauge this, a t-test was performed for the values that gave the largest standard deviation, that is the 100 μm runs (see Table 6). The six values were split into two groups of three, one group containing the three highest values and the other group with the three lowest. The test hypothesis that the difference in the average value of the two groups is zero results in t becoming equal to 2.55, thus the hypothesis is accepted at the 99.5% confidence limit. This worst case test suggests that six independent estimates provide a sufficient coverage of the range of possible V_{MD} values.

In section 4.2 (see also Table 7) it was noted that smaller particles tend to pack more closely than larger particles. If the spheres were close packed then ρ_r = 0.74 irrespective of particle size so it seems reasonable to assume that ρ_r should be independent of particle size (if all of the particles have the same radius in a given run) for a given mode of packing. The results in Table 7 suggest that the 30 μm particles pack in a different way to the 100 μm particles and this difference can be explained by the r^2 dependence of the terminal velocity. The smaller particles have a slower terminal velocity so they have more time to rearrange and adopt a more efficient packing structure than the larger particles. Alternatively, the difference could be due to the interparticle potential that might cause the interaction between particles to be radius dependent and thus affect the mode of packing. However, this is less likely since the form of this function and the method for choosing the parameters is the same, irrespective of particle radius.

The possibility of fractionation in the bimodal simulations is evident from the r^2 dependence of the terminal velocity. The larger particles tend to settle before the smaller particles because the larger particles have a higher terminal velocity. Plots of probability as a function of height for the mix simulations show the extent of fractionation. Each plot has a separate curve for every distinct particle size in the mix, therefore for the 30/50 μm simulation (Figure 4) there is one curve for the 30 μm particles and one for the 50 μm particles. The same applies for the 50/100 μm (Figure 5) and the 30/100 μm (Figure 6) simulations.

A common feature of these plots is a pair of well defined, sharp peaks at low heights. For example, the 30/50 μm plot (Figure 4) has a sharp peak at 26 μm for the 30 μm particles and another at 46 μm for the 50 μm particles. These peaks correspond to particles in contact with the floor of the container. The fact that these peaks occur at heights slightly lower than the corresponding particle radius indicate a small amount of overlap between the floor and the particles (i.e. squashing).

The tendency for the smaller particles to settle after the larger particles is shown by the plots. For the 30/50 μm simulation (Figure 4) the 30 μm probability curve extends out to 360 μm whereas the 50 μm curve only goes out to 310 μm. Thus, beyond 310 μm there is zero probability of finding a 50 μm particle and only 30 μm particles will be found in the range 310 μm to 360 μm, i.e. a layer of 30 μm particles will be formed on top of the sediment. Similarly, for the 50/100 μm simulation (Figure 5) 100 μm particles are not found above 578 μm and only 50 μm particles are found between 578 μm and 623 μm. The 30/100 μm simulation (Figure 6) is not as clear cut since the probability of finding a 100 μm particle above 470 μm is not zero but since it is very small we can take 470 as the upper limit for the

100 μm particles here. Only 30 μm particles will be found between 470 μm and 530 μm.

6. CONCLUSION

For a particle size distribution where the particles all have the same radius, the simulations indicate that the packing density is always less than the equivalent close packed structure. For a close packed structure $\rho_r = 0.74$ whereas the simulations gave $\rho_r = 0.72, 0.70, 0.68$ for particle radius of 30, 50, 100 μm respectively. Thus, the packing density was found to be particle size dependent; an increase in particle radius gave a decrease in sediment density. When the mix consists of particles of two distinct sizes, fractionation was found to occur. The larger particles have a higher terminal velocity than the smaller particles so they tend to settle before the smaller particles. This fractionation gives rise to a layer of smaller particles on the top of the sediment. This type of inhomogeneity has important consequences for the sensitivity and mechanical properties of an explosive where sedimentation may have occurred during production.

Understanding packing density for explosive fillers is important for explosive formulation, production and filling. The scope of the calculations presented in this paper has been limited by the computer time needed to perform the calculations. For example, approximately 22 hours of VAX 8700 CPU time is required to complete six runs of 200 particles (mixed sizes). In order to perform these calculations routinely and study larger systems (ie more complex particle size distributions and more particles), improvements in the time efficiency of the code will be essential. It is hoped that incorporating a vectorizable near-neighbours algorithm [6] into the code will allow a comprehensive series of calculations to be performed without too great a demand on computer resources.

7. ACKNOWLEDGEMENTS

The author would like to thank Dr. D.D. Richardson for providing the opportunity to undertake this work as well as providing expert advice on many aspects of the calculations. Thanks are also due to Mr. David Smith for assistance with random number generators and Mr. Ross Kummer for his continual assistance with various features of the MRL computer system and software packages. Finally, I would also like to thank Dr Dennis Evans for bringing to my attention the need to consider the effect of Brownian motion and Dr David Jones for his help with the Brownian motion effect.

8. REFERENCES

1. Parker, R.P. and Thorpe, B.W. (1970). The phase diagram of the RDX/TNT system (MRL Technical Note 140). Maribyrnong, Vic.: Materials Research Laboratory.

2. Van Gunsteren, W.F. and Berendsen, H.J.C. (1982). Molecular dynamics: Perspective for complex systems. Biochemical Society Transactions, **10**, 301-305

3. Marion, J.B. and Hornyak, W.F. (1982). Physics for science and engineering, International edition, chapter 5. Japan: Holt-Saunders.

4. Atkins, P.W. (1982). Physical Chemistry, second edition, 821-822. London: Oxford University Press.

5. Bossis, B. and Brady, J.F. (1984). Dynamic simulation of sheared suspensions. 1. General method. Journal of Chemical Physics, **80**, 5141-5154.

6. Verlet, L. (1967). Computer "experiments" on classical fluids. I. Thermodynamical properties of Lennard-Jones molecules. Physics Review, **159**, 98-103

7. Boris, J. (1986). A vectorized "near neighbours" algorithm of order N using a monotonic logical grid. Journal of Computational Physics, **66**, 1-20

8. Hammersley, J.M. and Handscomb, D.C. (1964). Monte Carlo methods, chapter 3. London: Methuen and Co Ltd.

9. Weast, R.C. (ed) (1983). CRC handbook of chemistry and physics, 64th edition, p F-38. Florida: CRC Press, Boca Raton.

10. Stoneham, A.M. and Taylor, R. (1981). Handbook of interatomic potentials II Metals (Report AERE-R 10205). Harwell: United Kingdom Atomic Energy Authority. Unclassified report.

11. Barth,H.G. (ed) (1984). Modern methods of particle size analysis, chapter 7. New York: John Wiley and Sons.

APPENDIX A

GLOSSARY OF SYMBOLS USED IN TEXT

η	liquid phase viscosity
r_i	radius of particle i
m_i	mass of i'th particle
$\mathbf{g}$	gravitational field strength.
r_{ij}	interparticle distance
ϵ_{ij} and σ_{ij}	Lennard-Jones constants for pair (i,j)
$\hat{\mathbf{d}}$	unit vector along the interparticle line
r_i^{floor}	distance between particle and bottom of container
K_i	particle/floor constant for particle type i
$\hat{\mathbf{k}}$	a unit vector in the Z direction
N	number of particles
v_i	particle i velocity
a_i	particle i acceleration
$v_i(t)$	velocity vector of particle i at time t
$a_i(t)$	acceleration vector of particle i at time t
$r_i(t)$	position vector of particle i at time t
x_n	particle i x-coord at time t
x_{n+1}	particle i x-coord at time=
x_{n-1}	particle i x-coord at time=
ρ_0	particle material density
$\mathbf{F_v}$	viscous force on particle i
$\mathbf{F_{ig}}$	gravitational force on particle i
$\mathbf{F_{ij}}$	interparticle force on particle i
$\mathbf{F}_i^{floor}$	particle/floor force on particle i
$\mathbf{F_i}$	total force on particle i

V_s	total volume of particles
V_c	close packed volume of spheres
V_{MD}	volume of sediment from MD simulation
ρ_{MD}	density of sediment from MD simulation
ρ_r	relative density of sediment to particle material
A	A is a constant
p(i)	p(i) is the i'th pseudo random number generated
M	M is the period of the pseudo random number generator

Table 1 ϵ values used in the interparticle force calculation for particles of radius 30, 50 and 100 μm.

	$\epsilon \times 10^{14}$ (J)		
	30	50	100
30	0.473	1.50	10.4
50	1.50	3.65	18.5
100	10.4	18.5	58.4

Table 2 σ values used in the interparticle force calculation for particles of radius 30, 50 and 100 μm.

	$\sigma \times 10^{5}$ (m)		
(m)	30	50	100
30	14.7	19.6	31.9
50	19.6	24.5	36.8
100	31.9	36.8	49.0

Table 3 K values used in the particle/floor force calculation

Radius (μm)	30	50	100
K ($N.m^{13}$)	3.54×10^{-68}	1.25×10^{-64}	8.22×10^{-60}

Table 4 Results for 30 μm particles simulation
Time step = 250 μs
Cycles = 6000
XY dimensions = 300 μm by 300 μm
Starting Z = 417 μm
Particle radius = 30 μm
No. of particles = 125

Run No.	V_{MD} (x 10^{-11} m^3)	Run time (mins)
1	1.969	45
2	1.976	43
3	1.970	42
4	1.970	42
5	1.978	42
6	1.970	46
Average	1.972	43
Std Dev	0.004	2

Table 5 Results for 50 μm particles simulation
Time step = 250 μs
Cycles = 6000
XY dimensions = 500 μm by 500 μm
Starting Z = 694 μm
Particle radius = 50 μm
No. of particles = 125

Run No.	V_{MD} (x 10^{-11} m^3)	Run time (mins)
1	9.41	45
2	9.49	43
3	9.38	41
4	9.00	41
5	9.21	42
6	9.60	42
7	9.08	40
Average	9.31	42
Std Dev	0.2	2

Table 6 Results for 100 μm particles simulation
Time step = 250 μs
Cycles = 6000
XY dimensions = 1000 μm by 1000 μm
Starting Z = 1389 μm
Particle radius = 100 μm
No. of particles = 125

Run No.	V_{MD} (x 10^{-11} m^3)	Run time (mins)
1	73.71	41
2	80.51	41
3	79.77	41
4	79.31	41
5	78.66	40
6	75.98	40
Average	78	41
Std Dev	2	0.5

Table 7 ρ_r values for the one-particle size distribution simulations

Radius (μm)	N	ρ_r
30	125	0.72
50	125	0.70
50	216	0.70
100	126	0.67

Table 8 Results for 50 μm particles simulation with an increased number of particles
Time step = 250 μs
Cycles = 6000
XY dimensions = 600 μm by 600 μm
Starting Z = 882 μm
Particle radius = 50 μm
No. of particles = 216

Run No.	V_{MD} (x 10^{-11} m^3)	Run time (mins)
1	15.80	117
2	15.80	127
3	16.41	128
4	16.43	128
5	16.33	118
6	16.41	129
Average	16.2	125
Std Dev	0.3	5

Table 9 Results for 30/50 μm particles mix simulation
Time step = 200 μs
Cycles = 12000
XY dimensions = 500 μm by 500 μm
Starting Z = 850 μm
Particle radius = 30 μm No. of particles = 125
Particle radius = 50 μm No. of particles = 75

Run No.	V_{MD} (x 10^{-11} m^3)	Run time (mins)
1	7.639	240
2	7.651	210
3	7.591	202
4	7.657	206
5	7.653	203
6	7.678	201
Average	7.65	210
Std Dev	0.03	14

Table 10: Results for 30/100 μm particles mix simulation
Time step = 150 μs
Cycles = 14000
XY dimensions = 1000 μm by 1000 μm
Starting Z = 1306 μm
Particle radius = 30 μm No. of particles = 125
Particle radius = 100 μm No. of particles = 75

Run No.	V_{MD} ($\times 10^{-11}$ m^3)	Run time (mins)
1	45.85	240
2	45.43	210
3	48.05	202
4	46.40	206
5	48.44	203
6	48.48	201
Average	47	237
Std Dev	1	9

Table 11: Results for 50/100 μm particles mix simulation
Time step = 200 μs
Cycles = 12000
XY dimensions = 1000 μm by 1000 μm
Starting Z = 1510 μm
Particle radius = 50 μm No. of particles = 125
Particle radius = 100 μm No. of particles = 75

Run No.	V_{MD} ($\times 10^{-11}$ m^3)	Run time (mins)
1	56.034	212
2	56.693	202
3	56.023	197
4	56.043	210
5	55.860	200
6	55.883	211
7	56.063	205
Average	55.9	205
Std Dev	0.1	5

Table 12 ρ_r values for the two-particle size distribution simulations

Radii (μm)	N	ρ_r
30/50	125/75	0.70
30/100	125/75	0.70
50/100	125/75	0.68

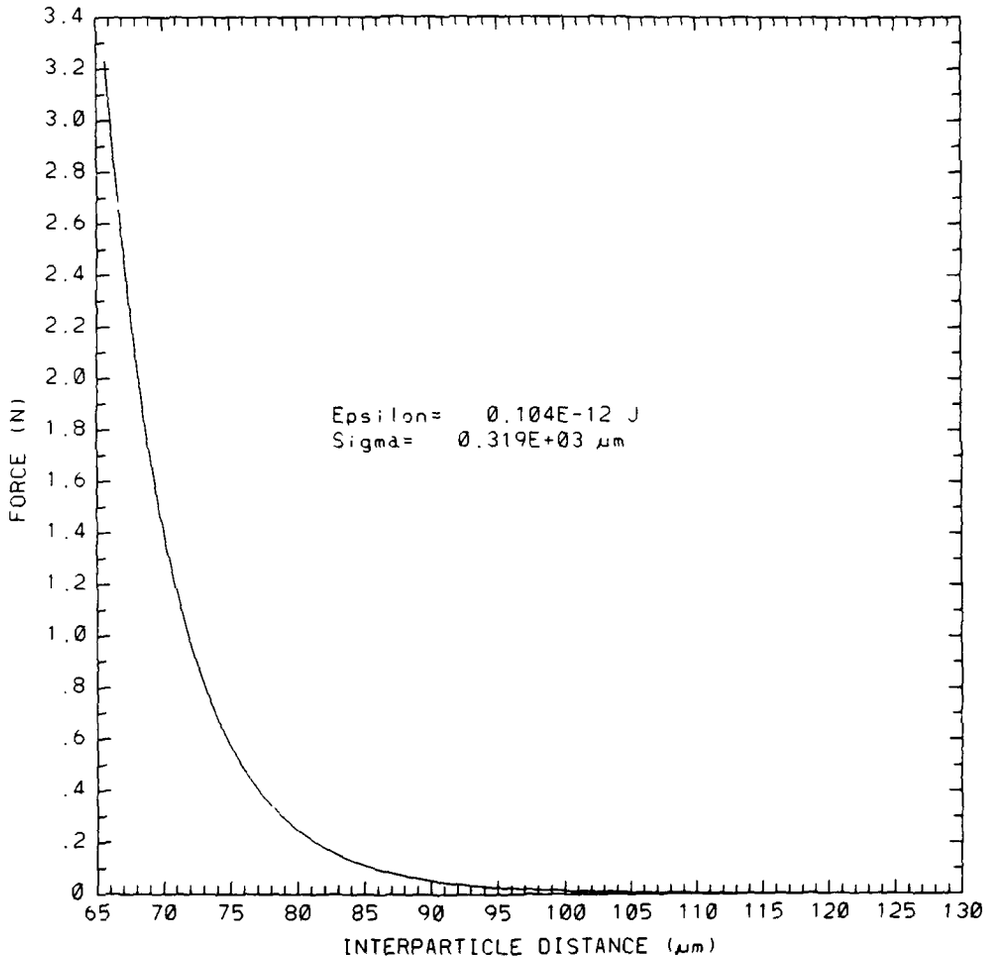

Figure 1 ***Force versus interparticle distance for 30/100 μm particle interaction, calculated using equation 3.***

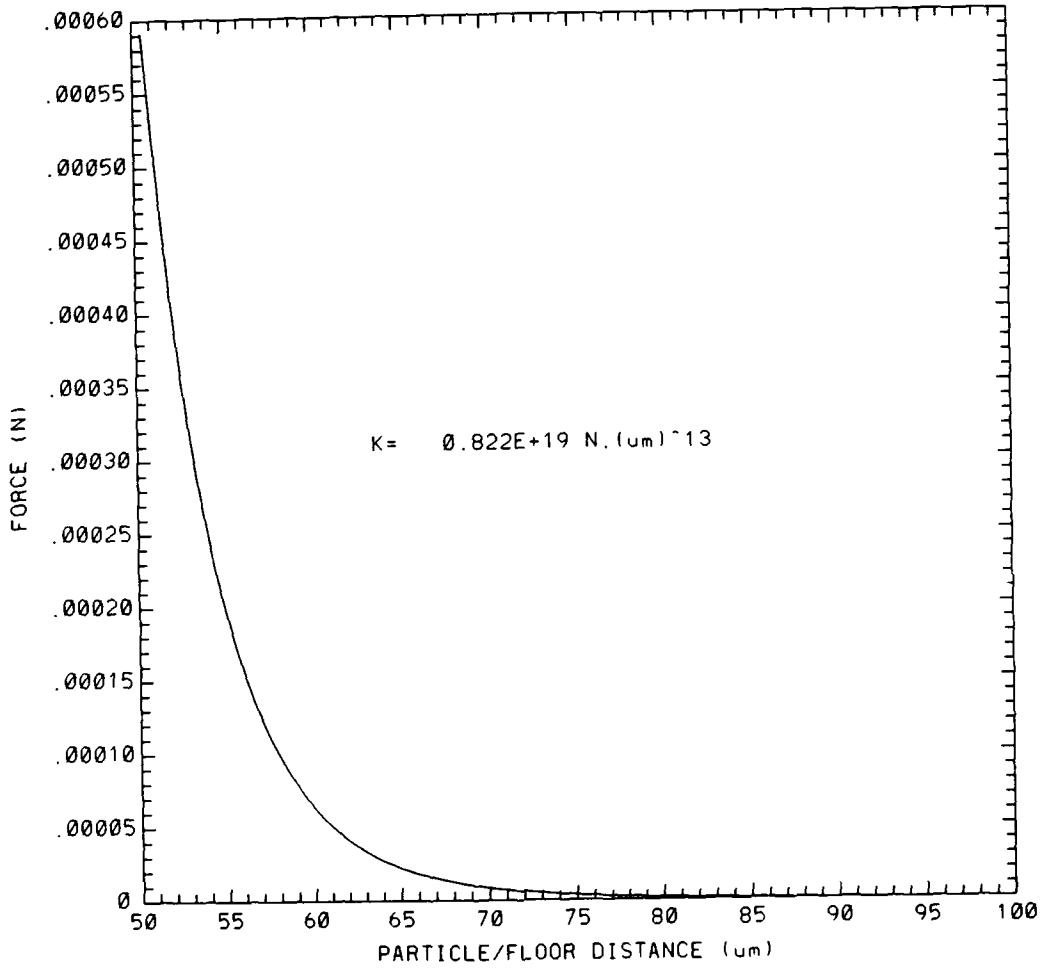

Figure 2 ***Force versus particle/floor distance for 100 μm particles and floor of container interaction, calculated using equation 4.***

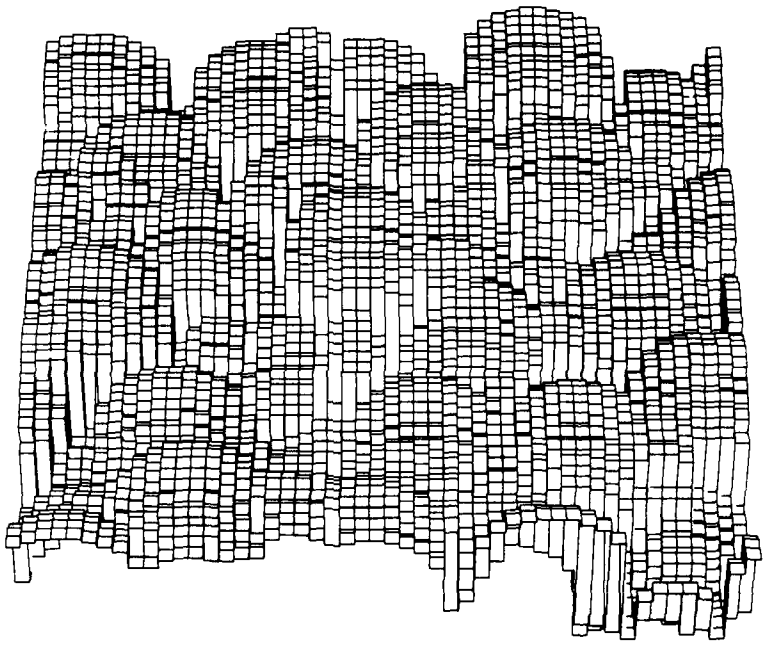

Figure 3 *Top surface of the sediment approximated by a grid of squares.*

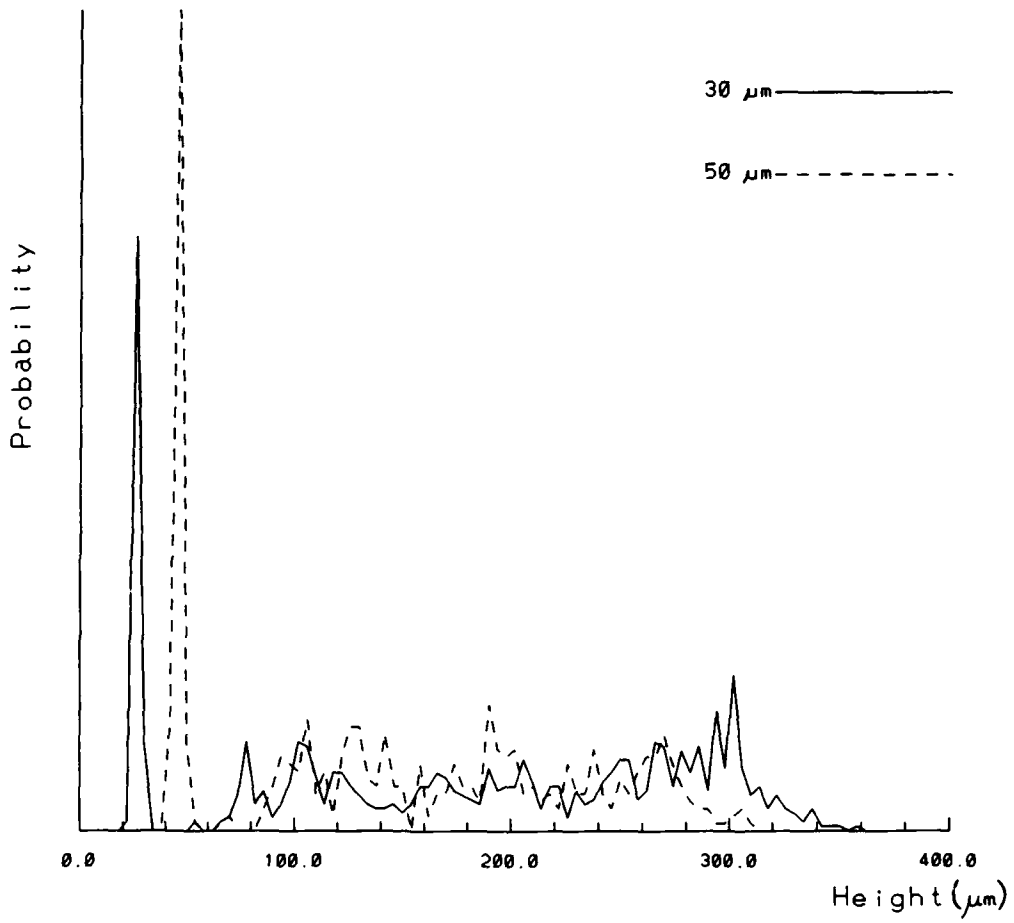

Figure 4 ***Probability of finding a particle as a function of particle height above the floor of the container for the 30/50 μm simulation. The solid line represents the probability curve for the 30 μm particles and the dashed line is the probability curve for the 50 μm particles.***

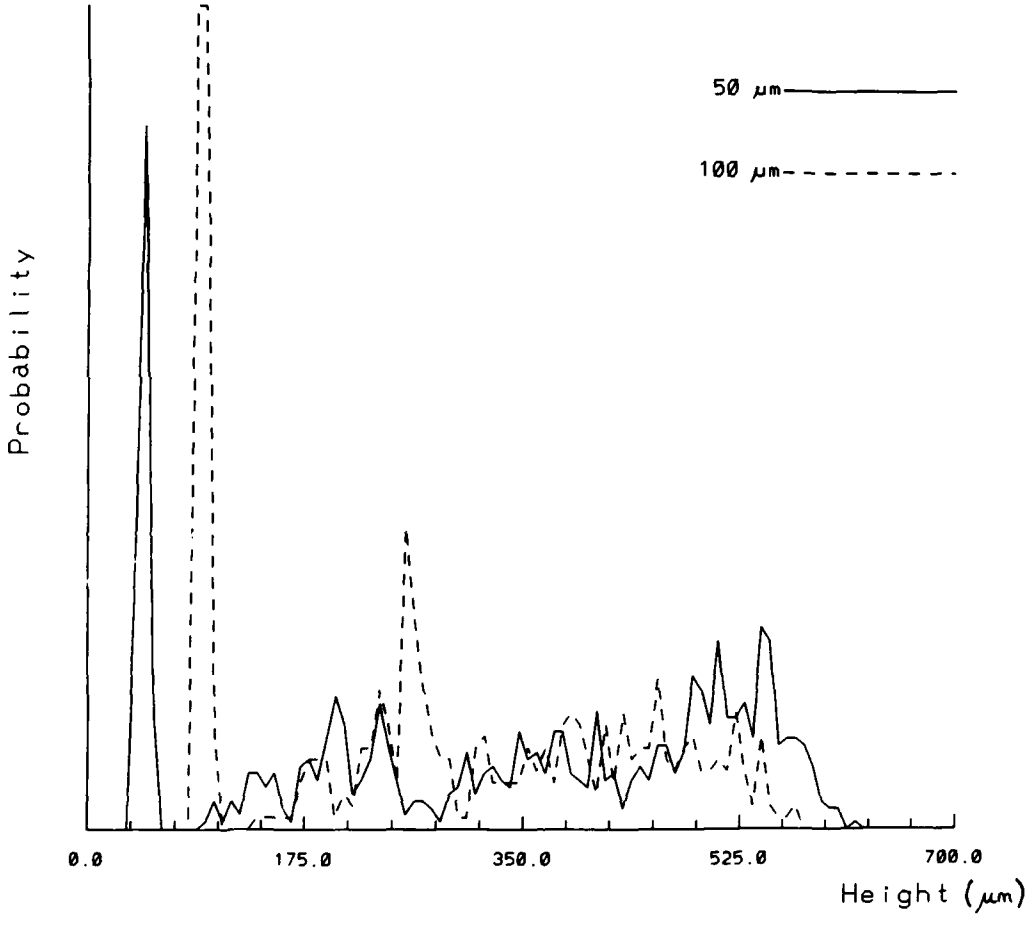

Figure 5 ***Probability of finding a particle as a function of particle height above the floor of the container for the 50/100 μm simulation. The solid line is for the 50 μm particles and the dashed line depicts the 100 μm particles.***

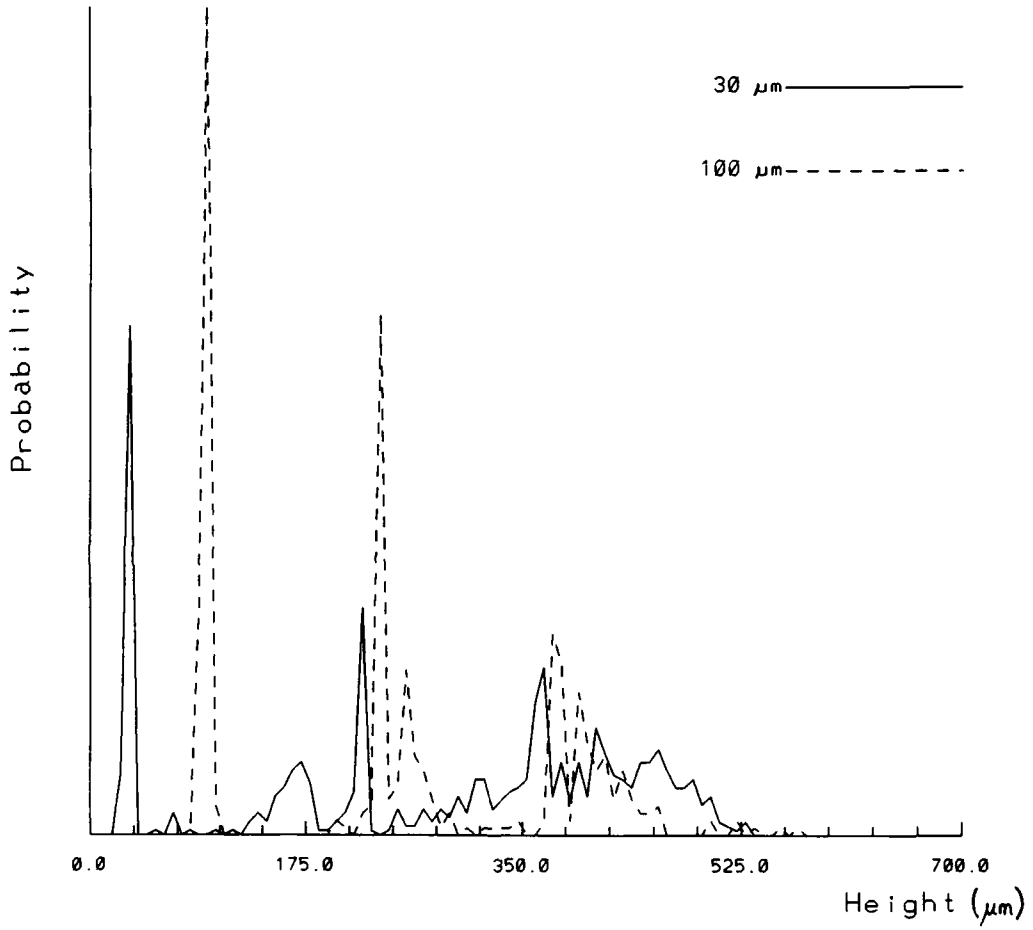

Figure 6 ***Probability of finding a particle as a function of particle height above the floor of the container for the 30/100 μm simulation. The solid line and the dashed line represent the probability curves for the 30 and 100 μm particles respectively.***

SECURITY CLASSIFICATION OF THIS PAGE **UNCLASSIFIED**

DOCUMENT CONTROL DATA SHEET

REPORT NO.	AR NO.	REPORT SECURITY CLASSIFICATION
MRL-RR-7-89	AR-005-733	Unclassified

TITLE

Simulation of sedimentation by molecular dynamics

AUTHOR(S)

Rodney A.J. Borg

CORPORATE AUTHOR

DSTO Materials Research Laboratory
PO Box 50
Ascot Vale Victoria 3032

REPORT DATE	TASK NO.	SPONSOR
August 1989		DSTO

FILE NO.	REFERENCES	PAGES
G6/4/8-3674	11	33

CLASSIFICATION/LIMITATION REVIEW DATE

CLASSIFICATION/RELEASE AUTHORITY

Chief, Explosives Division MRL

SECONDARY DISTRIBUTION

Approved for public release

ANNOUNCEMENT

Announcement of this report is unlimited

KEYWORDS

Composition B
RDX
TNT
Size separation
Particle size

SUBJECT GROUPS 0079A 0072E

ABSTRACT

A study of sedimentation processes of macroscopic, spherical particles using a molecular dynamics simulation was undertaken. Calculations were performed on particles of 30, 50 and 100 m radius. For particle size distributions where all of the particles have the same radius (monomodal) it was found that the density of the sediment is always less than the density of an equivalent close packed structure. In addition, an increase in particle radius leads to a decrease in the sediment density. For bimodal particle size mixes, either 30/50, 50/100 or 30/100 m radii, fractionation was found to occur. In all cases, the larger particles se'tled before the smaller particles giving rise to a layer of small particles on the top of the sediment, and a higher number ratio of larger particles in the lower portions.